Simple and Robust Algorithm for Multiphase Equilibrium Computations at Temperature and Volume Specifications

Chang Lu*, Zhehui Jin, Huazhou Li, and **Lingfei Xu****, University of Alberta

Summary

Two-phase and three-phase equilibria are frequently encountered in a variety of industrial processes, such as carbon dioxide (CO_2) injection for enhanced oil recovery in oil reservoirs, multiphase separation in surface separators, and multiphase flow in wellbores and pipelines. Simulation and engineering design of these processes using isothermal/isochoric (VT) multiphase equilibrium algorithms are sometimes more convenient than that using the conventional isothermal/isobaric (PT) algorithms. This work develops a robust algorithm for VT multiphase equilibrium calculations using a nested approach. The proposed algorithm is simple because a robust PT multiphase equilibrium algorithm is used in the inner loop without any further modifications, while an effective equation-solving method (i.e., Brent's method; Brent 1971) is applied in the outer loop to solve the pressure corresponding to a given volume/temperature specification. The robustness of the VT algorithm is safeguarded by using a highly efficient trust-region-method-based PT algorithm. We demonstrate the good performance of the newly developed algorithm by applying it to calculate the isochores of fluid mixtures that exhibit both two-phase and three-phase equilibria.

Introduction

In addition to two-phase equilibria, three-phase equilibria can be frequently observed in the upstream petroleum industry. For example, when CO_2 injection is applied to low-temperature reservoirs for enhanced oil recovery, gas/liquid/liquid three-phase equilibria can appear in the porous-media flow (Pan et al. 2015) or pipe flow (Pasqualette et al. 2020). In the steam-injection process for heavy-oil recovery, a different type of three-phase equilibria (i.e., gas/oil/water three-phase equilibria) can take place in the reservoir over a wide temperature/pressure range (Gao et al. 2017; Petitfrere et al. 2020). Hence, it is important to consider such three-phase equilibria in the compositional simulations of these processes (Pang and Li 2017; Connolly et al. 2019; Li and Li 2019; Petitfrere et al. 2020). Normally, engineers or researchers rely on the PT phase-equilibrium-calculation algorithms to perform the multiphase equilibrium computations for a given fluid mixture. In such algorithms, pressure, temperature, and feed composition are specified as inputs to the algorithm and the objective is to determine the number of equilibrium phases and their fractions, compositions, and volumes.

PT algorithms have been extensively studied for decades. Based on the two milestone works of Michelsen (1982a, 1982b), a sequential calculation framework consisting of stability tests and flash calculations becomes the convention for developing multiphase PT algorithms (Michelsen and Mollerup 2004; Firoozabadi 2015). For example, a three-phase PT equilibrium calculation starts with testing the stability of the given overall feed. If the feed composition is not stable, a two-phase flash is implemented. Then stability for one of the two phases is tested. If instability is observed again, a three-phase flash calculation is performed, and the phase fractions and phase compositions in the three-phase equilibrium are determined.

Numerous algorithms have been developed for stability tests and flash calculations. The classical algorithm for stability tests and flash calculations is the so-called successive-substitution (SS) method (Mehra et al. 1983; Li and Nghiem 1986; Ammar and Renon 1987). The SS method is usually used to provide the initial guess for higher-order algorithms such as Newton's method (Ammar and Renon 1987; Perschke 1988; Pan and Firoozabadi 2003; Hoteit and Firoozabadi 2006) and the trust-region method (Nghiem et al. 1983; Lucia and Feng 2003; Lucia et al. 2012; Petitfrere and Nichita 2014; Pan et al. 2019). Newton's method shows a fast convergence behavior with a good initial guess from SS, but convergence problems will be encountered under conditions along the stability test limit locus or in near-critical regions (Petitfrere and Nichita 2014). Petitfrere and Nichita (2014) suggest switching to the trust-region method when Newton's method fails. Using this idea, Pan et al. (2019) proposed a new multiphase PT algorithm combining the advantages of the three mentioned algorithms (i.e., SS, Newton, and trust-region methods). Specifically, the extensive tests performed by Pan et al. (2019) on nine CO_2 reservoir fluids show that there is no single failure encountered during the construction of pressure/composition (PX) phase diagrams involving both two-phase and three-phase equilibria.

Although algorithms with PT specifications have been extensively developed, the PT specification only represents a typical one among the specifications for multiple equilibrium calculations (Nagarajan et al. 1991; Michelsen 1999). Another important specification for working out the multiphase equilibrium problem is to use volume, temperature, and feed composition as the known information, and determine pressure, the number of equilibrating phases, and their properties (Michelsen 1999).

Such VT phase-equilibrium-calculation algorithms, or VT algorithms, have many practical and theoretical applications. A straightforward application is to aid the designing of storage tanks in the petroleum and chemical industry. Isochores and liquid-dropout curves can guide the design of the separation process (Cismondi et al. 2018). The VT algorithms can be also readily coupled into compositional reservoir/wellbore-flow simulators that are derived from a VT formulation (Polívka and Mikyška 2014). This new formulation in terms of VT specifications is proved to be robust and convenient. Several recent studies have further developed VT equilibrium calculation algorithms by taking into account the capillary pressure inside unconventional-rock nanopores (Sandoval et al. 2019; Achour and Okuno 2020, 2021). These studies show that the phase equilibrium calculations in VT space can be quite advantageous when considering the capillary pressure. Besides, VT algorithms can be applied to guide phase-behavior experiments in a fixed-volume pressure/volume/temperature (PVT) cell, as reported by Fontalba et al. (1984) and Kikani and Ratulowski (1998). For instance, a three-phase VT algorithm can be used to guide the fixed-volume three-phase-equilibrium measurements. In such fixed-volume experiments,

---

temperature is either increased or decreased. Then, the resulting pressure and phase volumes at equilibrium are measured. In the case of three-phase equilibrium tests, before the experiments, we need to design a feed composition that can induce the appearance of three-phase equilibria in the fixed-volume PVT cell. In such case, preliminary VT calculations can be conducted on a number of candidate feeds. On the basis of the VT calculation results, we can confidently select the ones that can result in the appearance of three-phase equilibria. Furthermore, VT algorithms can be potentially applied in the estimation of geological trapping pressures (Roedder and Bodnar 1980; Liu et al. 2003), thermodynamic equilibrium calculation considering gravity (Espósito et al. 2000), and other theoretical aspects (Cabral et al. 2005; Castier and Tavares 2005; Velez et al. 2010).

The natural way to solve the VT phase equilibrium problem is to recast it as a minimization of the Helmholtz free energy and solve the minimization problem using optimization routines. Mikyška and Firoozabadi (2011) defined new thermodynamic functions and developed a new VT algorithm using the new thermodynamic functions. Later, such an algorithm was successfully extended to three-phase equilibrium calculations (Jindrová and Mikyška 2013, 2015) and two-phase equilibrium calculations with the consideration of capillary pressure (Lu et al. 2019). Nichita (2018) developed a new unconstrained Helmholtz-free-energy minimization method used for conducting robust VT phase equilibrium calculations. At a given iteration level, Nichita (2018) treats volume as a variable dependent on mole numbers and solves such dependence with a nonlinear volume-balance equation. The algorithm is shown to be fast and robust. Nevertheless, it is not a trivial task to set up the VT algorithm code using the Helmholtz-free-energy minimization approach.

In view of the complexity of the Helmholtz-free-energy minimization approach, Cismondi et al. (2018) developed a simple but efficient VT algorithm for both vapor/liquid and liquid/liquid equilibria. Their VT algorithm is similar to the conventional PT algorithm framework proposed by Michelsen (1982a, 1982b), and the only difference is that under a guessed pressure, it solves the phase molar volumes by solving a pressure-equality equation. Cismondi et al. (2018) concluded that the phase equilibrium problem with VT specification can be treated as a problem of minimizing the Gibbs free energy with PT specification under a certain pressure-equality constraint. However, because the original two-phase PT algorithm is modified to be a VT algorithm, its robustness cannot be guaranteed when three-phase equilibria are encountered. This is why the VT algorithm by Cismondi et al. (2018) has difficulty in calculating the isochores that are within the three-phase region.

An alternative method would be approaching the VT phase equilibrium problem using an unaltered PT algorithm. Agarwal et al. (1991) developed such an algorithm to conduct isenthalpic equilibrium calculations with an embedded PT algorithm. In the Agarwal et al. (1991) algorithm, the PT algorithm is built in the inner loop, while temperature is solved in the outer loop to satisfy the energy-balance equation. Michelsen (1999) summarized a formal framework for formulating six specifications (such as pressure/enthalpy and VT specifications) for phase equilibrium computations. To solve the phase equilibrium problems with different specifications, Michelsen (1999) proposed a general solution framework that encompasses a Newton approach and a nested approach. The Newton approach solves all the unknowns using one loop. In the nested approach, a PT equilibrium is calculated in the inner loop, while the unknown variables are solved in the outer loop. Michelsen (1999) suggested two solution methods for solving the unknown variables in the nested approach: a second-order maximization method and a root-finding method. However, Michelsen (1999) did not further show how to numerically implement the root-finding method in the nested approach. Our experience indicates that the choice of the root-finding method can significantly affect the robustness and efficiency of the nested-approach-based VT algorithm. If the root-finding method is not properly selected, it can take hundreds of iterations to converge the VT algorithm. Therefore, it is of utmost importance to select a robust and efficient root-finding method to be used in the nested-approach-based VT algorithm.

The motivation of this work is to develop a robust, derivative-free, and easy-to-implement multiphase (up to three phases) VT equilibrium calculation algorithm that does not make any changes to the existing multiphase PT algorithm and directly calls the PT algorithm whenever needed. Such VT algorithm can be easily configured by practicing engineers to perform VT computations, provided a reliable PT algorithm is available. In the section Multiphase VT Algorithm, we introduce the methodology and numerical implementation of the nested approach for the multiphase VT calculations developed to solve for the isochores of a given fluid mixture. In the section Results and Discussion, we first demonstrate the robustness of the algorithm by examining its convergence behavior in the VT phase equilibrium calculations for two reservoir-fluid mixtures. We then present the isochore calculation results for two reservoir-fluid mixtures that exhibit single-phase, two-phase (including vapor/liquid and liquid/liquid), and three-phase (i.e., vapor/liquid/liquid) equilibria. We finally present the Conclusions section.

Multiphase VT Algorithm

Formulations for the Outer Loop. The VT phase equilibrium problem is a constrained minimization problem given by

$$\min \quad G(P, T, z), \quad\quad\quad\quad\quad\quad\quad\quad\quad\quad\quad\quad\quad\quad\quad\quad (1)$$

such that

$$V(P, T, z) - V_{\text{spec}} = 0, \quad\quad\quad\quad\quad\quad\quad\quad\quad\quad\quad\quad\quad (2)$$

where G represents the Gibbs free energy of the system and V and V_{spec} are the calculated molar volume and the user-specified molar volume, respectively. As suggested by Michelsen (1999), an easy-to-implement way to solve the problem defined by Eqs. 1 and 2 is to construct a nested approach where the minimum Gibbs free energy is found in the inner loop with a PT phase equilibrium algorithm. The calculated volume is updated in the outer loop by a root-finding algorithm to satisfy the equality constraint defined in Eq. 2.

To define the root-finding problem, Eq. 2 is transformed into a continuous function (f) given by

$$f(P, T, z) = V(P, T, z) - V_{\text{spec}}, \quad P^L < P < P^U, \quad\quad\quad\quad\quad\quad\quad\quad (3)$$

where P^L and P^U are the prespecified lower and upper pressure limits, respectively. The function values corresponding to P^L and P^U are represented by f^L and f^U, respectively. Note that P^L and P^U should guarantee $f^L \times f^U < 0$ such that a unique root exists in the interval $[P^L, P^U]$. The zero of the f function is then solved by a root-finding algorithm.

Root-Finding Algorithm. As one derivative-free root-finding algorithm, the secant method has been successfully used in isenthalpic flash algorithms (Agarwal et al. 1991; Li and Li 2017). One advantage of the secant method is that no derivative calculations are involved, although its speed is also compromised by this advantage. The secant method is applicable to our study because the isotherms in the pressure/volume space as described by a cubic equation of state are monotonic for multicomponent fluids (Firoozabadi 2015; Cismondi et al. 2018). However, the secant method can become unstable in the case of an inferior initial guess. To avoid this problem,

Dekker (1969) proposed a hybrid root-finding algorithm combining the bisection method and the secant method. Brent (1971) modified this algorithm to be a more stable and adaptable version. The algorithm proposed by Brent (1971) guarantees convergence in searching the zero of a function. It is a combination of the bisection method, the secant method, and the inverse quadratic interpolation method. In this study, we solve the root-finding problem defined in Eqs. 1 and 2 by Brent's method considering its robustness and efficiency (Brent 1971; Hoteit et al. 2006). Note that Brent's method was also adopted by Hoteit et al. (2006) for critical point calculations, demonstrating its superior performance. Appendix A gives a brief description of how to implement Brent's method in our multiphase VT algorithm.

Multiphase PT Algorithm for the Inner Loop. In this research, the PT algorithm is used to calculate the phase fractions and corresponding phase-compressibility factors in equilibrium. Then the value of f defined in Eq. 3 can be evaluated through Peng-Robinson equation of state (Robinson and Peng 1978). Petitfrere and Nichita (2014) and Pan et al. (2019) demonstrate that the trust-region-based optimization method is a highly efficient solution method for stability tests, multiphase flash calculations, and multiphase Rachford-Rice problems (Rachford and Rice 1952). For this reason, we choose the trust-region-based PT algorithm proposed by Pan et al. (2019) as the PT algorithm for the inner loop. This algorithm contains four key modules: one-phase stability test, two-phase flash calculation, two-phase stability test, and three-phase flash calculation modules. **Fig. 1** shows the detailed workflow of the PT algorithm proposed by Pan et al. (2019). Note that when the three-phase flash calculation fails for the first time, we choose the K-values associated with the second-lowest negative tangent-plane distance (TPD) value that resulted from the one-phase stability test.
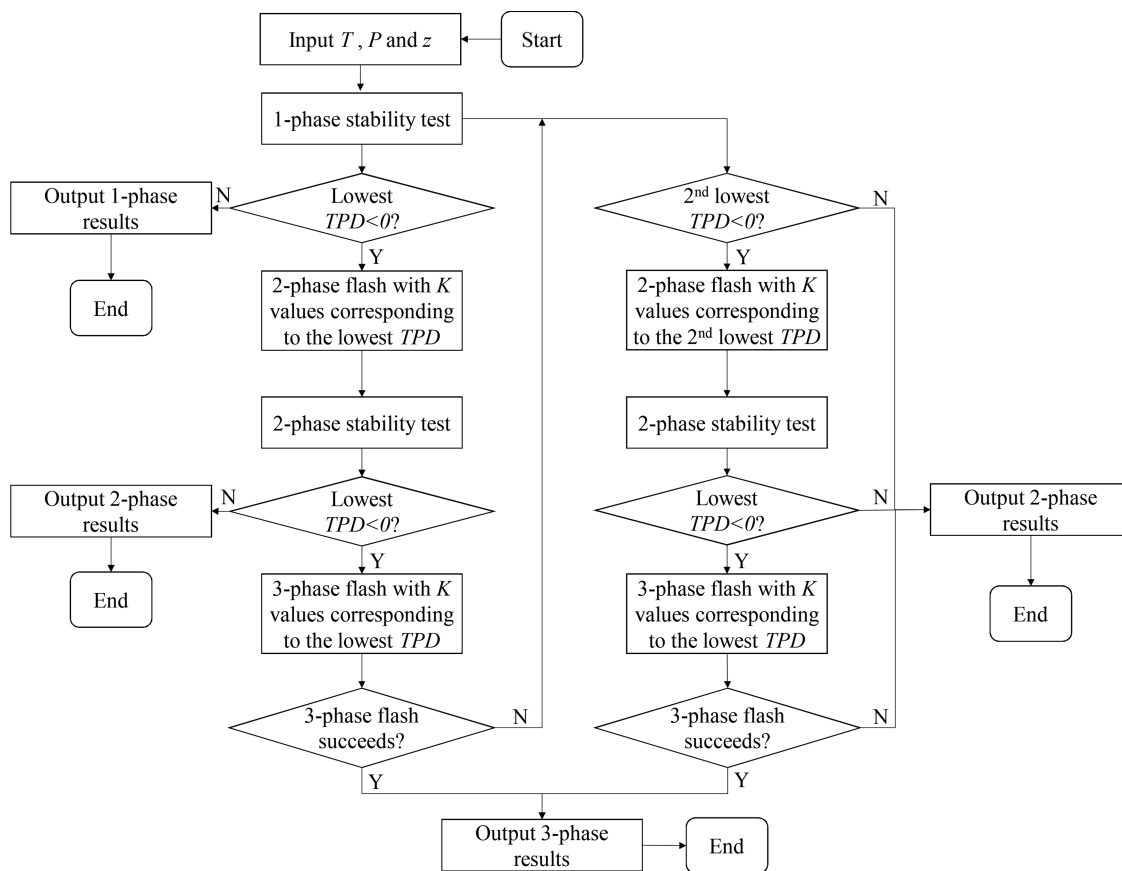

Fig. 1—Flow chart of the multiphase PT equilibrium calculation algorithm proposed by Pan et al. (2019).

For each key module mentioned previously, a sequential strategy (Petitfrere and Nichita 2014; Pan et al. 2019) is well-designed to ensure that the correct solution can be found for that module. The sequential strategy, which is first established by Petitfrere and Nichita (2014), is a consecutive execution process of three solvers. The classical SS method solver gives an acceptable initial convergence, Newton's solver provides a rapid convergence once the iteration point gets close to the solution, and the trust-region solver handles special cases where Newton's method encounters unfeasible conditions. A detailed coverage of how to apply the trust-region optimization method (Nocedal and Wright 2006) in the sequential strategy can be found in Petitfrere and Nichita (2014) and Pan et al. (2019).

For both one-phase and two-phase stability tests, the numbers of initial guesses in the algorithm of Pan et al. (2019) are largely reduced. This is done to accelerate the computational speed as much as possible for low-temperature reservoir fluids. In our applications, however, because the temperature range will be definitely larger, we use a total of $N_c + 5$ initial guesses for the one-phase stability test and $N_c + 6$ initial guesses for the two-phase stability test. The initial K-value estimations are given by (Michelsen 1982b; Li and Firoozabadi 2012; Pan et al. 2019)

$$K_i^{\text{Wilson}}, 1/K_i^{\text{Wilson}}, \sqrt[3]{K_i^{\text{Wilson}}}, 1/\sqrt[3]{K_i^{\text{Wilson}}}, K_i^{\text{pure}-j}, K_i^{\text{ideal}}, K_i^{\text{av}}, \dots\dots\dots\dots\dots\dots\dots\dots\dots\dots\dots\dots\dots\dots \quad (4)$$

where

$$K_i^{\text{Wilson}} = P_{c,i}\exp[5.37(1+\omega_i)(1-T_{c,i}/T)]/P, \dots\dots\dots\dots\dots\dots\dots\dots\dots\dots\dots\dots\dots\dots\dots \quad (5)$$

$$K_j^{\text{pure}-j} = 0.9/z_j, \; K_i^{\text{pure}-j} = 0.1/(N_c - 1)/z_i, \quad \dotfill \quad (6)$$

$$K_i^{\text{ideal}} = \hat{\phi}_i(z_i), \quad \dotfill \quad (7)$$

$$K_i^{\text{av}} = (x_i + y_i)/2, \quad \dotfill \quad (8)$$

and where $i \neq j$ and $i, j \in (1, 2, \cdots, N_c)$ and N_c is the total number of components. Note that K_i^{av} is only used in the two-phase stability test.

Algorithm Implementation. We develop a MATLAB® (The MathWorks, Inc., Natick, Massachusetts, USA) code for the proposed VT algorithm. **Fig. 2** shows its flow chart. To ensure $f^L \times f^U < 0$ in the interval $[P^L, P^U]$, P^L should be typically small (such as 1 bar) and P^U should be a relatively large value (such as 1,000 bar) so that the fluid is in one-phase condition. Besides, for a specified volume, one would like to know in advance whether the root exists in the interval. To find out this, we can numerically approximate a lower limit for the specified volume in the following manner: specify an initial V and check if $f^L \times f^U < 0$ holds; iteratively set $V = V - \Delta V$ and check if the inequality still holds. The calculation is terminated after $f^L \times f^U > 0$ and the approximated lower limit is then found for the specified volume. Conversely, if an "improper" small V is specified such that $f^L \times f^U > 0$ holds, we can iteratively set $V = V + \Delta V$ and check the inequality until $f^L \times f^U < 0$. The two preceding measures ensure that there is a unique root in the interval $[P^L, P^U]$ for the specified volume V.
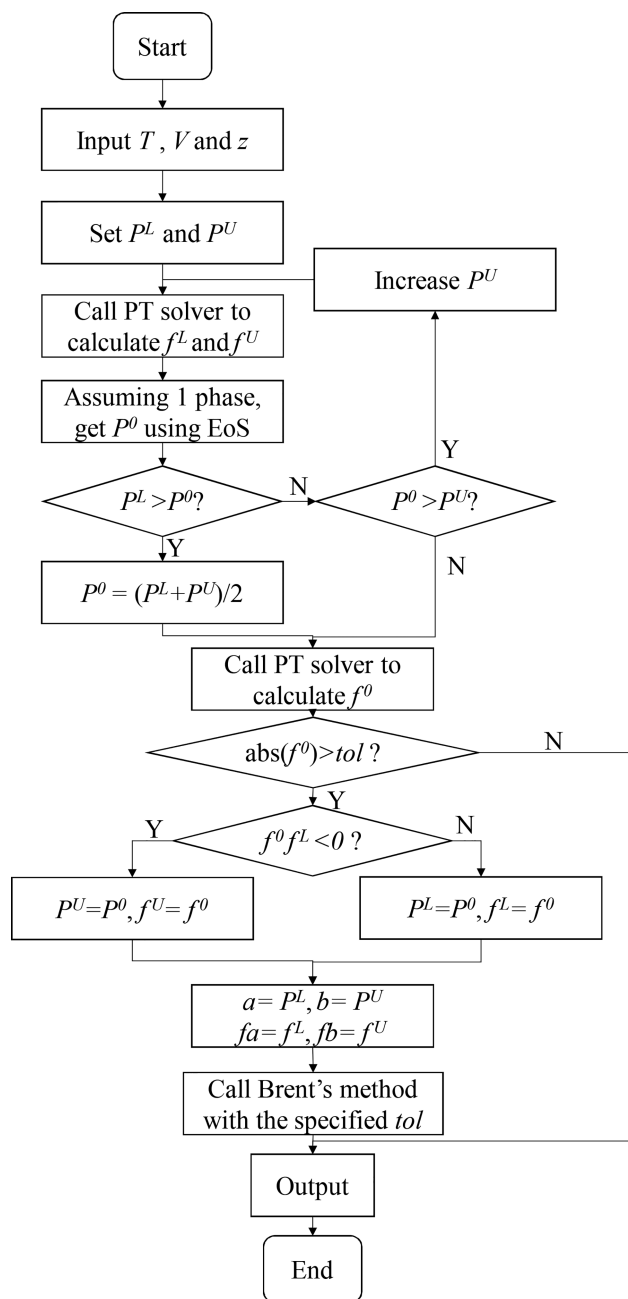

Fig. 2—Flow chart of the developed multiphase VT algorithm based on the multiphase PT algorithm proposed by Pan et al. (2019).

The following is the corresponding stepwise procedure executed in the multiphase VT algorithm:

1. Enter T, V, feed composition (z), and other fluid properties: critical temperature (T_c), critical pressure (P_c), acentric factors (ω), and binary-interaction parameters (BIPs).
2. Set the lower and upper boundaries of P (such as $P^L = 1$ bar and $P^U = 1000$ bar).
3. Call the PT algorithm to calculate f^L and f^U.
4. Assuming the fluid remains as one phase, calculate the initial guess P^0 using Peng-Robinson equation of state (Robinson and Peng, 1978).
5. If $P^L < P^0 < P^U$ is true, go to Step 7. If not, two options are available: if $P^0 < P^L$, set $P^0 = (P^L + P^U)/2$ and go to Step 7; if $P^0 > P^U$, go to Step 6.
6. Set $P^U = P^U + \Delta P$ and go back to Step 3. Note that ΔP is a user-defined increment such as 100 bar.
7. Calculate f^0 using Eq. 3 and check if abs(f^0) > tol (tol is a user-defined tolerance). If true, go to Step 8; if not, P^0 is the solution and go to Step 11.
8. Check if $f^0 \times f^L < 0$. If true, $P^U = P^0$ and $f^U = f^0$; if not, $P^L = P^0$ and $f^L = f^0$.
9. Set $a = P^L$, $b = P^U$, $fa = f^L$, $fb = f^U$ as the input parameters for Brent's method.
10. Call Brent's method, and record f and other essential parameters at the converged pressure $P = b$.
11. Output f, P, phase compositions, phase fractions, and phase-compressibility factors.

Results and Discussion

In this section, we discuss the multiphase-equilibrium-calculation results for four hydrocarbon fluids mixed with injection gases. The four hydrocarbon fluids are an acid gas (Pan and Firoozabadi 1998; Li and Firoozabadi 2012), Oil G (Khan et al. 1992; Pan et al. 2019), North Ward Estes (NWE) oil (Khan et al. 1992; Okuno et al. 2010), and JEMA oil (Khan et al. 1992; Okuno et al. 2010). Appendix B lists the properties of the four hydrocarbon fluids and the injection gases. Appendix C shows the four PX diagrams generated by running the trust-region-based PT algorithm. No single failure is found during construction of these diagrams.

Next, we examine the convergence behavior of the newly developed VT algorithm. Finally, two detailed case studies are conducted to calculate the isochores that involve one-phase, two-phase, and three-phase equilibria.

Convergence Behavior. We compare the convergence behavior of three versions of VT algorithms that are generated by using the three equation-searching methods: Brent's method, the secant method, and the bisection method. Note that the residual of the function value is defined as abs(f) and the termination criterion used in the VT algorithms is abs(f) < tol = 1×10^{-6}. For comparative analysis, we select several points on the phase boundaries or in the near-critical regions of the PX diagram for the acid gas case (Appendix C, Fig. C-1), and the PT and PX diagrams for the Oil G case (**Fig. 3** and Fig. C-2). **Table 1** shows the selected five points and their corresponding conditions.

No.	Fluid	Location on Phase Diagram	Pressure (bar)	Temperature (K)	Injected CO_2 Fraction (mol%)	Estimated Volume (cm³/mol)
1	Acid gas	Three-phase boundary	39.0125	178.80	47.0	40.4546
2	Acid gas	Two-phase boundary	13.4375	178.80	92.2	33.5512
3	Oil G	Three-phase near-critical region	77.20	307.59	98.6	102.4006
4	Oil G	Two-phase near-critical region	307.00	315.50	70.0	76.7663
5	Oil G	Three-phase near-critical region	90.40	314.00	70.0	99.6498

Table 1—Selected study points and their corresponding conditions used in the convergence study.
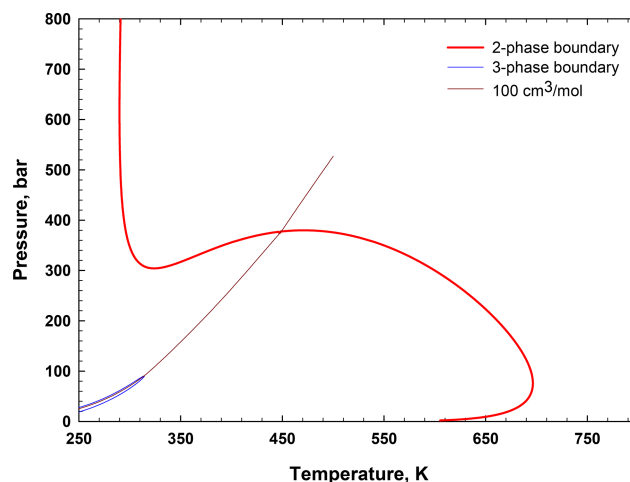

Fig. 3—Two-phase envelope, three-phase envelope, and the isochoric line of 100 cm³/mol calculated for Oil G mixed with 70 mol% injection gas.

Figs. 4 through 8 compare the convergence behavior of the three VT algorithms at the selected points. **Table 2** shows the corresponding computation time. The calculations are performed in MATLAB using a desktop personal computer with Intel® Core i7-3770 (Intel Corporation, Santa Clara, California, USA) central processing unit @3.4 GHz and with 12 GB RAM. In general, it can be seen from Figs. 4 through 8 and Table 2 that Brent's method appears to be the most robust and efficient method among the three methods. The bisection method is also robust but computationally more expensive than Brent's method. The secant method exhibits two different patterns of convergence behavior. In the first pattern, the secant method can quickly converge to the solution (Figs. 4, 6, and 7). In the other pattern, the secant method only converges to the solution after an excessive number of iterations (Figs. 5 and 8). We can also conclude from Figs. 4 through 8 and Table 2 that Brent's method strikes a good balance between robustness and efficiency because Brent's method is a well-designed hybrid method that could switch to the most suitable method during iteration.
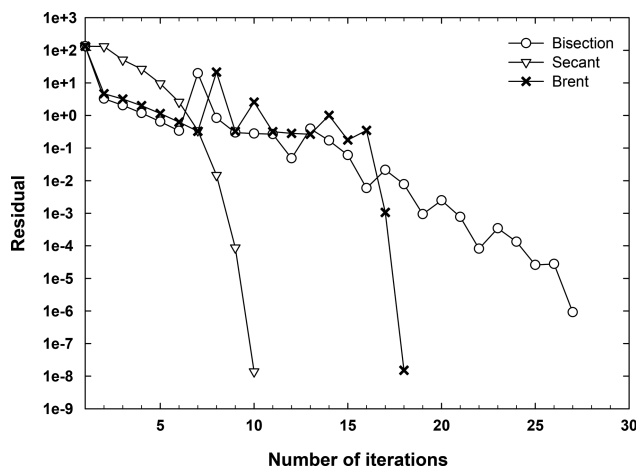
Fig. 4—Convergence behavior of Brent's method, secant method, and bisection method in the VT algorithms at 40.4546 cm³/mol and 178.8 K for the acid gas case. The VT condition corresponds to a point at 39.0125 bar and 47.0 mol% of injected CO_2 on the three-phase boundary line in Fig. C-1.
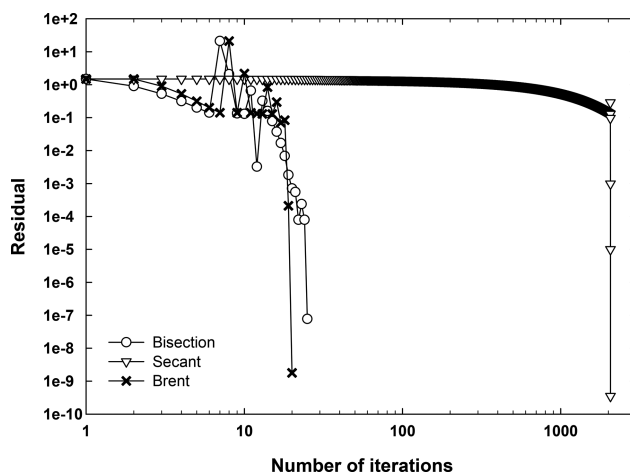

Fig. 5—Convergence behavior of Brent's method, secant method, and bisection method in the VT algorithms at 33.5512 cm³/mol and 178.8 K for the acid gas case. The VT condition corresponds to a point at 13.4375 bar and 92.2 mol% of injected CO_2 on the two-phase boundary line in Fig. C-1.

Fig. 9 shows the convergence behavior of the three algorithms along an isochore. This isochore is at 100 cm³/mol in the PT space for the Oil G sample mixed with 70 mol% of pure CO_2. Fig. 3 shows the corresponding phase envelopes calculated by the PT algorithm and the isochore discussed here. Note that in Fig. 9, there are some points with one PT algorithm call because the values of f^0 at these one-phase points directly satisfy the termination condition. The number of the PT algorithm calls tends to increase when the number of equilibrating phases increases from one to two, as well as from two to three. As can be seen from Fig. 9, Brent's method shows the smallest average number of PT algorithm calls along the isochore from 250 to 500 K, followed by the bisection method. The two patterns of convergence behavior exhibited by the secant method can also be observed in Fig. 9. Specifically, in the two-phase region at relatively high temperatures, the number of PT algorithm calls by secant method remains as low as Brent's method. When the temperature decreases to 328 K, the average number of PT algorithm calls required by the secant method abruptly jumps to 403.

Isochoric Computations. We show the calculation results for two case studies. The first case study is focused on the three-phase equilibrium calculations for the NWE oil sample mixed with 70 mol% of an impure CO_2 mixture (i.e., CO_2/methane mixture), while the second case study is focused on the three-phase equilibrium calculations for the JEMA oil sample mixed with 75 mol% of pure CO_2. Both mixtures exhibit three-phase vapor/liquid/liquid equilibria at low temperatures (Khan et al. 1992). In this subsection, we only show the calculation results for the NWE oil, while Appendix D shows the calculation results for the JEMA oil.
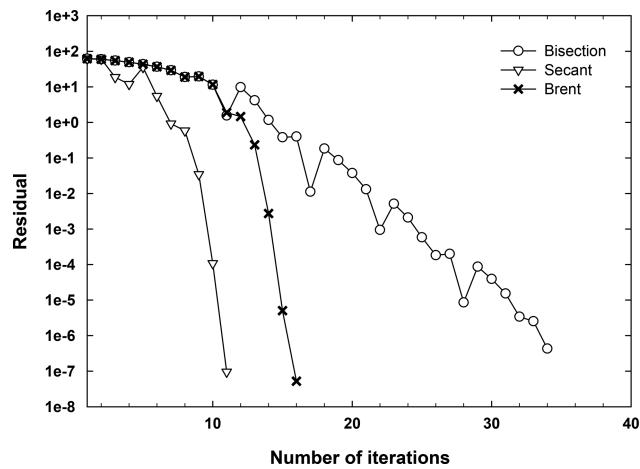
Fig. 6—Convergence behavior of Brent's method, secant method, and bisection method in the VT algorithms at 102.4006 cm³/mol and 307.59 K for Oil G. The VT condition corresponds to a point at 77.2 bar and 98.6 mol% of injected CO_2 in the three-phase near-critical region of Fig. C-2.
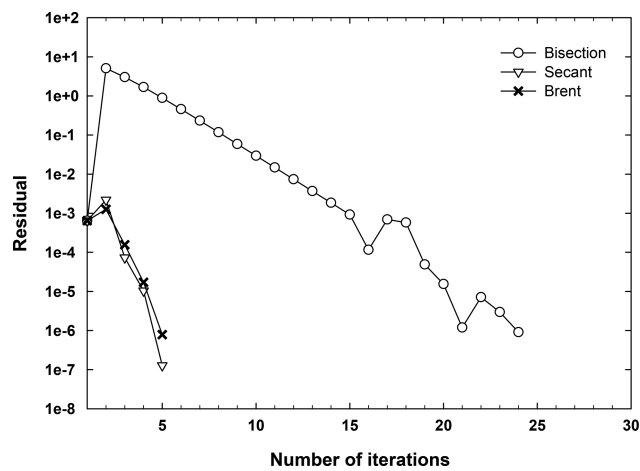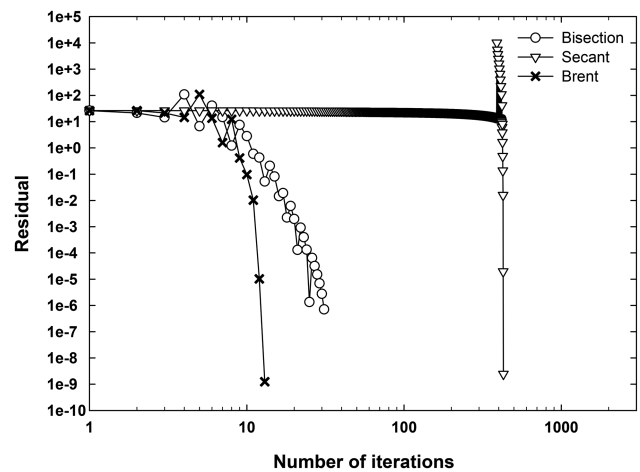

Fig. 7—Convergence behavior of Brent's method, secant method, and bisection method in the VT algorithms at 76.7663 cm³/mol and 315.5 K for Oil G. The VT condition corresponds to a point at 307 bar and 315.5 K in the two-phase near-critical region of Fig. 3.

Fig. 8—Convergence behavior of Brent's method, secant method, and bisection method in the VT algorithms at 99.6498 cm³/mol and 314 K for Oil G. The VT condition corresponds to a point at 90.4 bar and 314 K in the three-phase near-critical region of Fig. 3.

We first calculate the PT phase envelopes for the NWE oil mixed with 70 mol% injection gas using the PT algorithm. **Fig. 10** shows the calculation results. As temperature reduces (see Fig. 10), the bubblepoint curve of the two-phase envelope is uplifted to the extremely high-pressure side of the phase diagram, instead of showing a downward trend as exhibited by the commonly seen reservoir fluids. This is reminiscent of a liquid/liquid immiscibility phenomenon (Michelsen 1982b). Because of the liquid/liquid immiscibility, one tiny three-phase vapor/liquid/liquid equilibrium region appears at the lower-left corner of the diagram. In Fig. 10 are also drawn the

isochoric lines at constant molar volumes (ranging from 80 to 500 cm^3/mol) that are computed with the proposed VT algorithm. These isochoric lines are generated by repetitively performing the VT calculations under a constant molar volume but gradually reducing temperature. Note that no single failure occurs during the VT computations along all the isochores shown in Fig. 10. As a part of Fig. 10, **Fig. 11** shows an enlarged view of the three-phase envelope together with the isochoric lines passing through the three-phase region. Liquid/liquid equilibria reside above the three-phase envelope, while vapor/liquid equilibria prevail below the three-phase envelope. As can be seen from Figs. 10 and 11, starting from the one-phase equilibria at higher pressures, all the isochoric lines tend to first encounter the two-phase envelope and then pass through the three-phase envelope. Another interesting observation from Fig. 11 is that the slope change of the isochoric lines transitioning from a liquid/liquid equilibrium to a vapor/liquid/liquid equilibrium is much more abrupt than that exhibited by the isochoric lines transitioning from one vapor/liquid equilibrium to a vapor/liquid/liquid equilibrium.

No.	Fluid	Location on Phase Diagram	Brent's Method (seconds)	Secant Method (seconds)	Bisection Method (seconds)
1	Acid gas	Three-phase boundary	6.201	4.889	9.973
2	Acid gas	Two-phase boundary	2.821	77.610	4.247
3	Oil G	Three-phase near-critical region	7.865	6.691	16.710
4	Oil G	Two-phase near-critical region	4.614	6.682	11.609
5	Oil G	Three-phase near-critical region	5.740	132.013	17.289
		Average	5.448	45.577	11.966

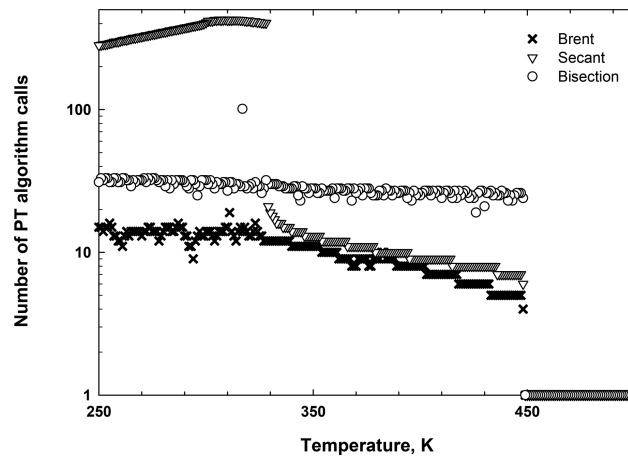Table 2—Computation time at the selected points consumed by the three VT algorithms.

Fig. 9—Number of PT algorithm calls required by Brent's method, secant method, and bisection method in the VT algorithms along an isochore of 100 cm^3/mol for the Oil G sample mixed with 70 mol% of pure CO_2.
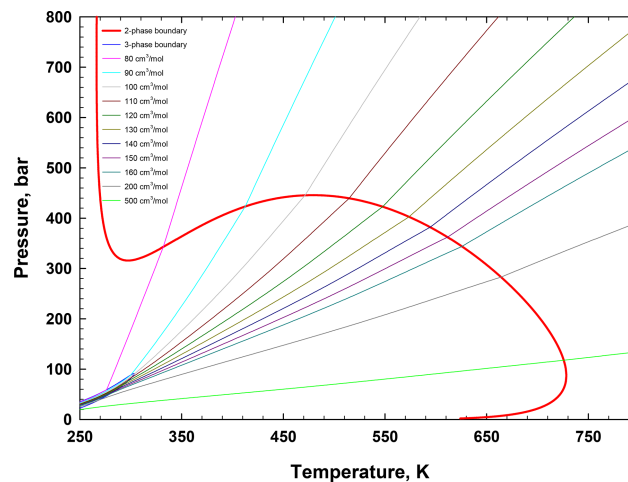

Fig. 10—Two-phase and three-phase envelopes calculated for the NWE oil mixed with 70-mol% injection gas as shown in Appendix B, Table B-3. The isochoric lines, calculated with the proposed VT algorithm, are also shown.
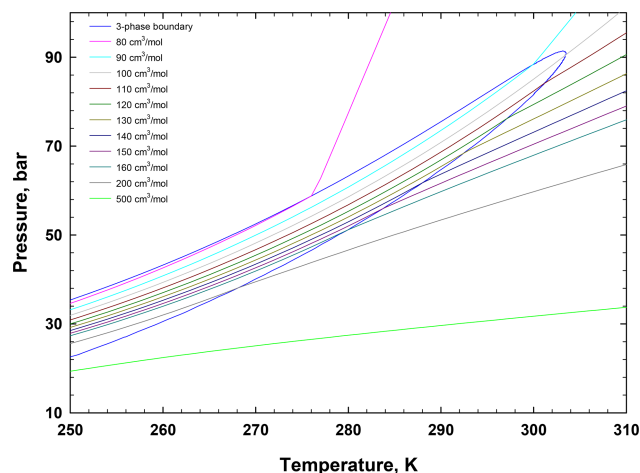
Fig. 11—Close-up view showing the three-phase boundary with the isochoric lines passing through the three-phase region for the NWE oil mixed with 70 mol% injection gas.

In addition, one can observe an interesting feature exhibited by Figs. 10 and 11: All the isochores tend to trace back to the three-phase region. This implies that if one conducts VT phase equilibrium calculations along a given isochore, it is highly likely for one to sequentially encounter single-phase, two-phase, and three-phase equilibria. This becomes advantageous because one could initialize a three-phase-envelope construction algorithm by locating the intersection between the isochore and the three-phase boundary. This is one of the motivations underlying the development of density-based algorithms for constructing phase envelopes, as attempted by Nichita (2019). Such a method of using a given isochore for initializing three-phase-envelope tracing algorithms is different from the conventional approach (Michelsen 1980; Lindeloff and Michelsen 2003; Venkatarathnam 2014; Agger and Sørensen 2018; Cismondi 2018). **Fig. 12** shows a projection of the two-phase and three-phase envelopes (shown in Fig. 10) in the temperature/molar-volume space, while **Fig. 13** shows the same projection in the temperature/density space. These phase boundaries are tracked using the isochoric flash results calculated by the VT algorithm developed in this study. Similar charts are displayed in Molina et al. (2019) and Nichita (2019). Nichita (2019) showed that the density-based calculation method can be readily applied to generate two-phase boundaries in the temperature/density space.
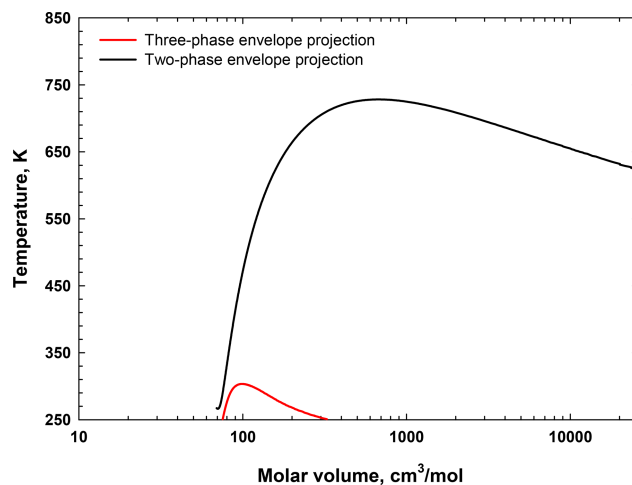

Fig. 12—Projection of two-phase and three-phase envelopes in the temperature/molar-volume space calculated for the NWE oil mixed with 70 mol% injection gas.

Isochoric calculations can reveal how the phase fractions vary as a function of temperature in a fixed-volume cell. **Fig. 14** illustrates how the phase fractions vary as temperature reduces along an isochoric line of $80\,cm^3/mol$. Along this isochoric line, the phase equilibria switch from single liquid-phase equilibria to liquid/liquid two-phase equilibria and, finally, to vapor/liquid/liquid three-phase equilibria. Note that the dashed curves for two- and three-phase boundaries in Fig. 14 are located at 332 and 276 K, respectively. **Fig. 15** illustrates how the phase fractions vary as temperature reduces along an isochoric line with a much larger molar volume of $120\,cm^3/mol$. In a slightly different way, the phase equilibria switch from single vapor-phase equilibria to vapor/liquid two-phase equilibria and, finally, to vapor/liquid/liquid three-phase equilibria. The dashed curves for two- and three-phase boundaries are located at 547 and 297 K, respectively.

Fig. 16 shows the number of PT algorithm calls in the VT algorithm computations along the isochore of $120\,cm^3/mol$. Similar to the observation in Fig. 9, the number of PT algorithm calls in Fig. 16 increases with the increase in the number of equilibrating phases. Along the isochore, the maximum number of the PT algorithm calls is 15 from 250 K to 800 K. **Fig. 17** further shows a statistical summary of the number of PT algorithm calls during the VT algorithm computations for all the isochores shown in Fig. 10. Fig. 17 shows that, on average, approximately 6.1 calls are required to converge the VT algorithm. The average number becomes 9.07 if we exclude the points with one PT algorithm call. Results in Figs. 16 and 17 demonstrate a good overall efficiency of the proposed VT algorithm.
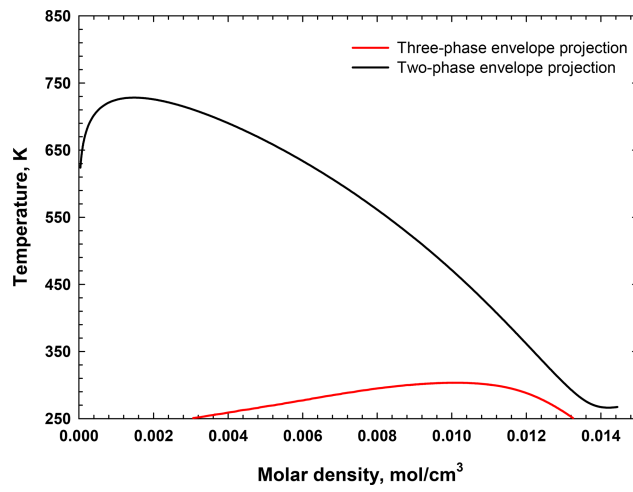
Fig. 13—Projection of two-phase and three-phase envelopes in the temperature/density space calculated for the NWE oil mixed with 70-mol% injection gas.
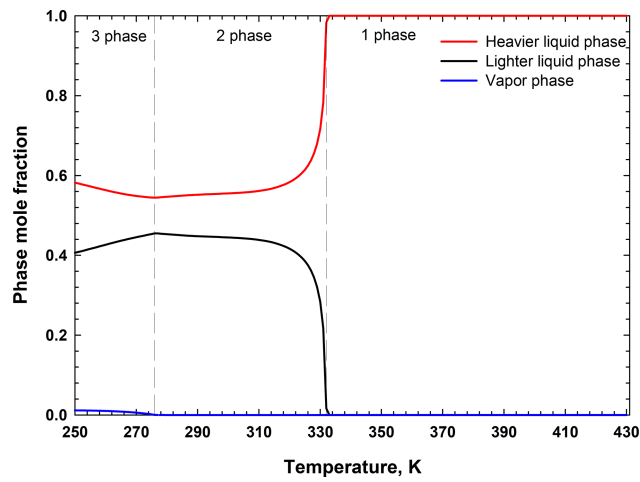

Fig. 14—Variation of phase fractions vs. temperature along the isochore of 80 cm³/mol calculated for the NWE oil mixed with 70-mol% injection gas.
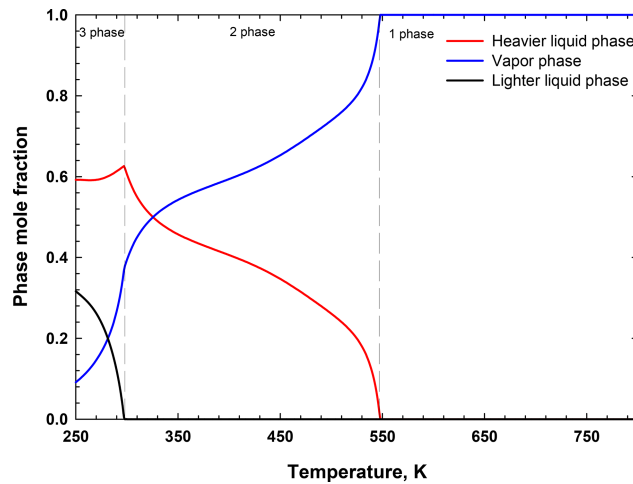

Fig. 15—Variation of phase fractions vs. temperature along the isochore of 120 cm³/mol for the NWE oil mixed with 70-mol% injection gas.
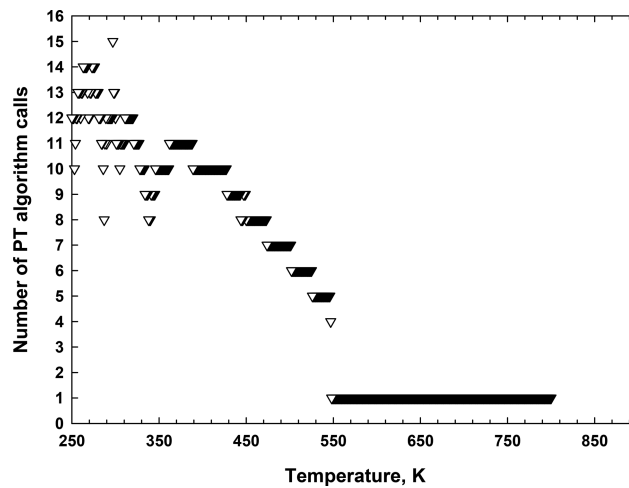
Fig. 16—Number of PT algorithm calls in the implementation of the VT algorithm along the isochore of 120 cm³/mol for the NWE oil mixed with 70-mol% injection gas.
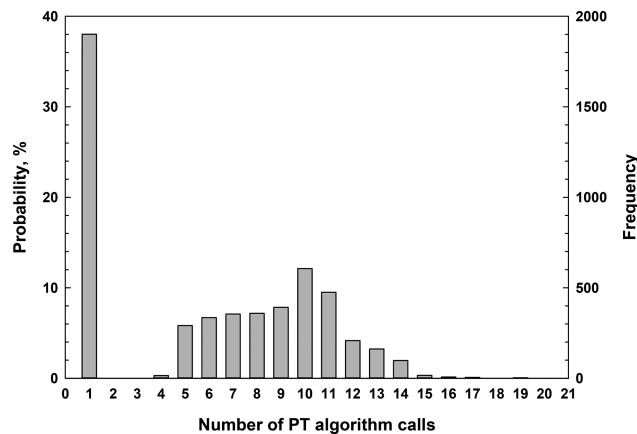

Fig. 17—Statistical summary of the number of PT algorithm calls in the implementation of the VT algorithm along the isochores shown in Fig. 10.

Conclusions

In this work, we develop a robust and simple VT algorithm for conducting multiphase equilibrium calculations, especially for CO_2-inclusive mixtures. We draw the following conclusions from the present study:

1. The multiphase VT algorithm is built using a nested approach. The multiphase PT algorithm is embedded as the inner loop without any further modifications, while an effective equation-solving algorithm (i.e., Brent's method) is applied in the outer loop to solve for the pressure corresponding to a given volume/temperature specification.
2. The robustness of the newly developed VT algorithm is safeguarded with the combined use of the trust-region-method-based PT algorithm and Brent's method. These two algorithms are shown to be very robust in previous studies as well as in the present study.
3. Our example calculations on several fluid mixtures demonstrate that the new VT algorithm is always able to converge to the correct phase equilibria, including one-phase equilibria, vapor/liquid or liquid/liquid two-phase equilibria, and vapor/liquid/liquid three-phase equilibria.
4. The new algorithm is shown to be relatively efficient. On average, fewer than 10 times of the PT algorithm calls are required to converge the VT algorithm calculations for two-phase and three-phase equilibria.
5. The potential applications of the developed VT algorithm are multifold. In particular, the VT algorithm presented in this study can be potentially leveraged to provide reliable initializations in the phase-envelope-construction algorithm. We will try to develop a new phase-envelope-construction algorithm using the developed multiphase VT algorithm as one of our future works.

Nomenclature

a, b, c, d, e = independent variables; i.e., pressure values for the proposed VT algorithm
eps = machine precision used in Brent's method
f = continuous function, defined by Eq. 3
fa, fb, fc = function values calculated at a, b, c using Eq. 3
G = Gibbs free energy
K^{av} = average K-value estimation used in two-phase stability test
K^{pure} = K-value estimation of corner point corresponding to a near-pure trial phase
K^{ideal} = K-value estimation considering ideal gas law
K^{Wilson} = K-value estimation calculated by Wilson correlation
m, p, q, r, s = intermediate variables in Brent's method
N_c = total number of components

P = pressure, bar
P_c = critical pressure, bar
t = positive tolerance defined in Brent's method
tol = error tolerance
T = temperature, K
T_c = critical temperature, K
V = molar volume, cm^3/mol
V_{spec} = specified molar volume, cm^3/mol
x = liquid-like phase composition
y = vapor-like phase composition
z = feed composition
ω = acentric factor
$\hat{\phi}$ = fugacity coefficient

Subscript

i, j = component index

Superscripts

j = component index
L = lower limit
U = upper limit
0 = initial guess

Acknowledgments

References

Achour, S. H. and Okuno, R. 2020. Phase Stability Analysis for Tight Porous Media by Minimization of the Helmholtz Free Energy. *Fluid Phase Equilib* **520** (1 October): 112648. https://doi.org/10.1016/j.fluid.2020.112648.

Achour, S. H. and Okuno, R. 2021. Two-Phase Flash for Tight Porous Media by Minimization of the Helmholtz Free Energy. *Fluid Phase Equilib* **534** (15 April): 112960. https://doi.org/10.1016/j.fluid.2021.112960.

Agarwal, R. K., Li, Y. K., Nghiem, L. X. et al. 1991. Multiphase Multicomponent Isenthalpic Flash Calculations. *J Can Pet Technol* **30** (3): 69–75. PETSOC-91-03-07. https://doi.org/10.2118/91-03-07.

Agger, C. S. and Sørensen, H. 2018. Algorithm for Constructing Complete Asphaltene PT and Px Phase Diagrams. *Ind. Eng. Chem. Res.* **57** (1): 392–400. https://doi.org/10.1021/acs.iecr.7b04246.

Ammar, M. N. and Renon, H. 1987. The Isothermal Flash Problem: New Methods for Phase Split Calculations. *AIChE J* **33** (6): 926–939. https://doi.org/10.1002/aic.690330606.

Brent, R. P. 1971. An Algorithm with Guaranteed Convergence for Finding a Zero of a Function. *Comput J* **14** (4): 422–425. https://doi.org/10.1093/comjnl/14.4.422.

Cabral, V. F., Castier, M., and Tavares, F. W. 2005. Thermodynamic Equilibrium in Systems with Multiple Adsorbed and Bulk Phases. *Chem Eng Sci* **60** (6): 1773–1782. https://doi.org/10.1016/j.ces.2004.11.007.

Castier, M. and Tavares, F. W. 2005. Centrifugation Equilibrium of Natural Gas. *Chem Eng Sci* **60** (11): 2927–2935. https://doi.org/10.1016/j.ces.2004.12.027.

Cismondi, M. 2018. Phase Envelopes for Reservoir Fluids with Asphaltene Onset Lines: An Integral Computation Strategy for Complex Combinations of Two- and Three-Phase Behaviors. *Energy Fuels* **32** (3): 2742–2748. https://doi.org/10.1021/acs.energyfuels.7b02790.

Cismondi, M., Ndiaye, P. M., and Tavares, F. W. 2018. A New Simple and Efficient Flash Algorithm for T-v Specifications. *Fluid Phase Equilib* **464** (25 May): 32–39. https://doi.org/10.1016/j.fluid.2018.02.019.

Connolly, M., Pan, H., and Tchelepi, H. 2019. Three-Phase Equilibrium Computations for Hydrocarbon-Water Mixtures Using a Reduced Variables Method. *Ind. Eng. Chem. Res.* **58** (32): 14954–14974. https://doi.org/10.1021/acs.iecr.9b00695.

Dekker, T. J. 1969. Finding a Zero by Means of Successive Linear Interpolation. In *Constructive Aspects of the Fundamental Theorem of Algebra*, ed. B. Dejon and P. Henrici, 37–48. Hoboken, New Jersey, USA: Wiley-Interscience.

Espósito, R. O., Castier, M., and Tavares, F. W. 2000. Calculations of Thermodynamic Equilibrium in Systems Subject to Gravitational Fields. *Chem Eng Sci* **55** (17): 3495–3504. https://doi.org/10.1016/S0009-2509(00)00010-5.

Firoozabadi, A. 2015. *Thermodynamics and Applications of Hydrocarbon Energy Production*. New York, New York, USA: McGraw-Hill Education.

Fontalba, F., Richon, D., and Renon, H. 1984. Simultaneous Determination of Vapor-Liquid Equilibria and Saturated Densities Up to 45 MPa and 433 K. *Rev Sci Instrum* **55** (6): 944–951. https://doi.org/10.1063/1.1137870.

Gao, J., Okuno, R., and Li, H. 2017. An Experimental Study of Multiphase Behavior for *n*-Butane/Bitumen/Water Mixtures. *SPE J*. **22** (3): 783–798. SPE-180736-PA. https://doi.org/10.2118/180736-PA.

Hoteit, H. and Firoozabadi, A. 2006. Simple Phase Stability-Testing Algorithm in the Reduction Method. *AIChE J* **52** (8): 2909–2920. https://doi.org/10.1002/aic.10908.

Hoteit, H., Santiso, E., and Firoozabadi, A. 2006. An Efficient and Robust Algorithm for the Calculation of Gas-Liquid Critical Point of Multicomponent Petroleum Fluids. *Fluid Phase Equilib* **241** (1–2): 186–195. https://doi.org/10.1016/j.fluid.2005.12.019.

Jindrová, T. and Mikyška, J. 2013. Fast and Robust Algorithm for Calculation of Two-Phase Equilibria at Given Volume, Temperature, and Moles. *Fluid Phase Equilib* **353** (15 September): 101–114. https://doi.org/10.1016/j.fluid.2013.05.036.

Jindrová, T. and Mikyška, J. 2015. General Algorithm for Multiphase Equilibria Calculation at Given Volume, Temperature, and Moles. *Fluid Phase Equilib* **393** (15 May): 7–25. https://doi.org/10.1016/j.fluid.2015.02.013.

Khan, S. A., Pope, G. A., and Sepehrnoori, K. 1992. Fluid Characterization of Three-Phase CO$_2$/Oil Mixtures. Paper presented at the SPE/DOE Enhanced Oil Recovery Symposium, Tulsa, Oklahoma, USA, 22–24 April. SPE-24130-MS. https://doi.org/10.2118/24130-MS.

Kikani, J. and Ratulowski, J. 1998. Consistency Check and Reconciliation of PVT Data from Samples Obtained with Formation Testers Using EOS Models. *SPE Res Eval & Eng* **1** (4): 348–353. SPE-50979-PA. https://doi.org/10.2118/50979-PA.

Li, Z. and Firoozabadi, A. 2012. General Strategy for Stability Testing and Phase-Split Calculation in Two and Three Phases. *SPE J.* **17** (4): 1096–1107. SPE-129844-PA. https://doi.org/10.2118/129844-PA.

Li, R. and Li, H. 2017. A Robust Three-Phase Isenthalpic Flash Algorithm Based on Free-Water Assumption. *J. Energy Resour. Technol.* **140** (3): 032902. https://doi.org/10.1115/1.4037901.

Li, R. and Li, H. 2019. Improved Three-Phase Equilibrium Calculation Algorithm for Water/Hydrocarbon Mixtures. *Fuel* **244** (15): 517–527. https://doi.org/10.1016/j.fuel.2019.02.026.

Li, Y. K. and Nghiem, L. X. 1986. Phase Equilibria of Oil, Gas and Water/Brine Mixtures from a Cubic Equation of State and Henry's Law. *Can J Chem Eng* **64** (3): 486–496. https://doi.org/10.1002/cjce.5450640319.

Lindeloff, N. and Michelsen, M. L. 2003. Phase Envelope Calculations for Hydrocarbon-Water Mixtures. *SPE J.* **8** (3): 298–303. SPE-85971-PA. https://doi.org/10.2118/85971-PA.

Liu, D. H., Xiao, X. M., Mi, J. K. et al. 2003. Determination of Trapping Pressure and Temperature of Petroleum Inclusions Using PVT Simulation Software—A Case Study of Lower Ordovician Carbonates from the Lunnan Low Uplift, Tarim Basin. *Mar Pet Geol* **20** (1): 29–43. https://doi.org/10.1016/S0264-8172(03)00047-3.

Lu, C., Jin, Z., and Li, H. 2019. A Two-Phase Flash Algorithm with the Consideration of Capillary Pressure at Specified Mole Numbers, Volume and Temperature. *Fluid Phase Equilib* **485** (15 April): 67–82. https://doi.org/10.1016/j.fluid.2018.12.002.

Lucia, A., Bonk, B. M., Waterman, R. R. et al. 2012. A Multi-Scale Framework for Multi-Phase Equilibrium Flash. *Comput Chem Eng* **36** (10 January): 79–98. https://doi.org/10.1016/j.compchemeng.2011.07.01.

Lucia, A. and Feng, Y. 2003. Multivariable Terrain Methods. *AIChE J* **49** (10): 2553–2563. https://doi.org/10.1002/aic.690491010.

Mehra, R. K., Heidemann, R. A., and Aziz, K. 1983. An Accelerated Successive Substitution Algorithm. *Can J Chem Eng* **61** (4): 590–596. https://doi.org/10.1002/cjce.5450610414.

Michelsen, M. L. 1980. Calculation of Phase Envelopes and Critical Points for Multicomponent Mixtures. *Fluid Phase Equilib* **4** (1–2): 1–10. https://doi.org/10.1016/0378-3812(80)80001-X.

Michelsen, M. L. 1982a. The Isothermal Flash Problem. Part I. Stability Test. *Fluid Phase Equilib* **9** (1): 1–19. https://doi.org/10.1016/0378-3812(82)85001-2.

Michelsen, M. L. 1982b. The Isothermal Flash Problem. Part II. Phase-Split Calculation. *Fluid Phase Equilib* **9** (1): 21–40. https://doi.org/10.1016/0378-3812(82)85002-4.

Michelsen, M. L. 1999. State Function Based Flash Specifications. *Fluid Phase Equilib* **158–160** (June): 617–626. https://doi.org/10.1016/S0378-3812(99)00092-8.

Michelsen, M. L. and Mollerup, J. M. 2004. *Thermodynamic Models: Fundamentals and Computational Aspects*. Holte, Denmark: Tie-Line Publications.

Mikyška, J. and Firoozabadi, A. 2011. A New Thermodynamic Function for Phase-Splitting at Constant Temperature, Moles, and Volume. *AIChE J.* **57** (7): 1897–1904. https://doi.org/10.1002/aic.12387.

Molina, M. J., Rodriguez-Reartes, S. B., and Zabaloy, M. S. 2019. Computation and Analysis of Binary Multiphase Isochors. *Fluid Phase Equilib* **500** (15 November): 112227. https://doi.org/10.1016/j.fluid.2019.06.017.

Nagarajan, N. R., Cullick, A. S., and Griewank, A. 1991. New Strategy for Phase Equilibrium and Critical Point Calculations by Thermodynamic Energy Analysis. Part I. Stability Analysis and Flash. *Fluid Phase Equilib* **62** (3): 191–210. https://doi.org/10.1016/0378-3812(91)80010-S.

Nghiem, L. X., Aziz, K., and Li, Y. K. 1983. A Robust Iterative Method for Flash Calculations Using the Soave-Redlich-Kwong or the Peng-Robinson Equation of State. *SPE J.* **23** (3): 521–530. SPE-8285-PA. https://doi.org/10.2118/8285-PA.

Nichita, D. V. 2018. New Unconstrained Minimization Methods for Robust Flash Calculations at Temperature, Volume and Moles Specifications. *Fluid Phase Equilib* **466** (25 June): 31–47. https://doi.org/10.1016/j.fluid.2018.03.

Nichita, D. V. 2019. A Simple Approximate Density-Based Phase Envelope Construction Method. *Fluid Phase Equilib* **499** (1): 112245. https://doi.org/10.1016/j.fluid.2019.112245.

Nocedal, J. and Wright, S. J. 2006. *Numerical Optimization*, second edition. New York, New York, USA: Springer Series in Operations Research, Springer Science+Business Media.

Okuno, R., Johns, R., and Sepehrnoori, K. 2010. Three-Phase Flash in Compositional Simulation Using a Reduced Method. *SPE J.* **15** (3): 689–703. SPE-125226-PA. https://doi.org/10.2118/125226-PA.

Pan, H., Chen, Y., Sheffield, J. et al. 2015. Phase-Behavior Modeling and Flow Simulation for Low-Temperature CO_2 Injection. *SPE Res Eval & Eng* **18** (2): 250–263. SPE-170903-PA. https://doi.org/10.2118/170903-PA.

Pan, H., Connolly, M., and Tchelepi, H. 2019. Multiphase Equilibrium Calculation Framework for Compositional Simulation of CO_2 Injection in Low-Temperature Reservoirs. *Ind. Eng. Chem. Res.* **58** (5): 2052–2070. https://doi.org/10.1021/acs.iecr.8b05229.

Pan, H. and Firoozabadi, A. 1998. Complex Multiphase Equilibrium Calculations by Direct Minimization of Gibbs Free Energy by Use of Simulated Annealing. *SPE Res Eval & Eng* **1** (1): 36–42. SPE-37689-PA. https://doi.org/10.2118/37689-PA.

Pan, H. and Firoozabadi, A. 2003. Fast and Robust Algorithm for Compositional Modeling: Part II—Two-Phase Flash Computations. *SPE J.* **8** (4): 380–391. SPE-71603-MS. https://doi.org/10.2118/71603-MS.

Pang, W. and Li, H. 2017. An Augmented Free-Water Three-Phase Flash Algorithm for CO_2/Hydrocarbon/Water Mixtures. *Fluid Phase Equilib* **450** (25 October): 86–98. https://doi.org/10.1016/j.fluid.2017.07.010.

Pasqualette, M. D., Carneiro, J., Johansen, S. T. et al. 2020. A Numerical Assessment of Carbon-Dioxide-Rich Two-Phase Flows with Dense Phases in Offshore Production Pipelines. *SPE J.* **25** (2): 712–731. SPE-199876-PA. https://doi.org/10.2118/199876-PA.

Perschke, D. R. 1988. *Equation of State Phase Behavior Modeling for Compositional Simulation*. PhD dissertation, University of Texas at Austin, Austin, Texas, USA.

Petitfrere, M. and Nichita, D. V. 2014. Robust and Efficient Trust-Region Based Stability Analysis and Multiphase Flash Calculations. *Fluid Phase Equilib* **362** (25 January): 51–68. https://doi.org/10.1016/j.fluid.2013.08.039.

Petitfrere, M., Nichita, D. V., Voskov, D. et al. 2020. Full-EoS Based Thermal Multiphase Compositional Simulation of CO_2 and Steam Injection Processes. *J Pet Sci Eng* **192** (September): 107241. https://doi.org/10.1016/j.petrol.2020.107241.

Polívka, O. and Mikyška, J. 2014. Compositional Modeling in Porous Media Using Constant Volume Flash and Flux Computation Without the Need for Phase Identification. *J Comput Phys* **272** (1 September): 149–169. https://doi.org/10.1016/j.jcp.2014.04.029.

Rachford, H. Jr. and Rice, J. 1952. Procedure for Use of Electronic Digital Computers in Calculating Flash Vaporization Hydrocarbon Equilibrium. *J Pet Technol* **4** (10): 19. SPE-952327-G. https://doi.org/10.2118/952327-G.

Robinson, D. B. and Peng, D. Y. 1978. *The Characterization of the Heptanes and Heavier Fractions for the GPA Peng-Robinson Programs*. Tulsa, Oklahoma, USA: Gas Processors Association.

Roedder, E. and Bodnar, R. J. 1980. Geologic Pressure Determinations from Fluid Inclusion Studies. *Ann. Rev. Earth Planet. Sci.* **8** (1): 263–301. https://doi.org/10.1146/annurev.ea.08.050180.001403.

Sandoval, D. R., Michelsen, M. L., Yan, W. et al. 2019. VT-Based Phase Envelope and Flash Calculations in the Presence of Capillary Pressure. *Ind. Eng. Chem. Res.* **58** (13): 5291–5300. https://doi.org/10.1021/acs.iecr.8b05976.

Velez, A., Pereda, S., and Brignole, E. A. 2010. Isochoric Lines and Determination of Phase Transitions in Supercritical Reactors. *J Supercrit Fluids* **55** (2): 643–647. https://doi.org/10.1016/j.supflu.2010.09.033.

Venkatarathnam, G. 2014. Density Marching Method for Calculating Phase Envelopes. 2. Three-Phase Envelopes. *Ind. Eng. Chem. Res.* **53** (30): 12122–12128. https://doi.org/10.1021/ie501838y.

Appendix A—Numerical Implementation of Brent's Method

Fig. A-1 shows a flow chart of Brent's method (Brent 1971). In Fig. A-1, the parameters a, b, c, d, and e are values of the independent variables, which are pressure values in our problem. The parameters fa, fb, and fc are function values calculated at a, b, and c using Eq. 3. The parameters m, p, q, r, and s are intermediate variables. The finally calculated value of b is the solution of our problem. As shown in Fig. A-1, two error tolerances, namely tol_1 and tol_2, are defined. In Brent's definition, tol_1 is defined for b as

$$tol_1 = 2 \times \text{eps} \times |b| + t, \dots\dots\dots\dots\dots\dots\dots\dots\dots\dots\dots\dots\dots\dots\dots\dots \text{(A-1)}$$

where t is a positive tolerance and eps is the machine precision. In the implementation, one can pay more attention to the function value fb, because $fb=0$ means we find the root. Herein, we define tol_2 as a user-defined tolerance that directly corresponds to the function value fb. We then set $tol_1 \ll tol_2$ so that the only active termination criterion of the algorithm is $\text{abs}(fb) \leq tol_2$. In the main text, tol_2 is directly represented instead by tol.
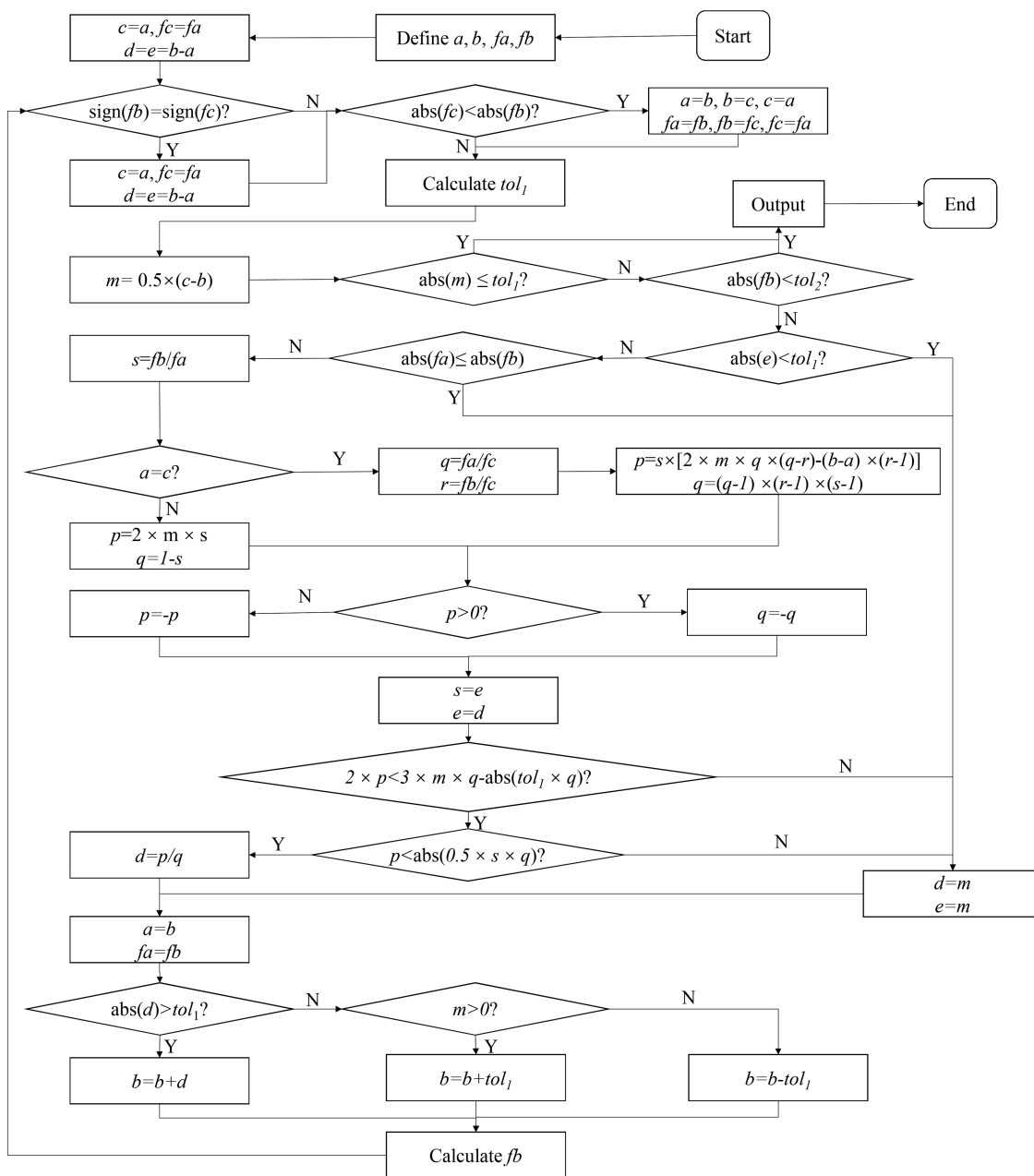

Fig. A-1—Flow chart of Brent's root-finding method (Brent 1971).

Appendix B—Properties of Hydrocarbon Fluids and Injected Gases

Please see **Tables B-1 through B-4.**

Components	Oil Composition (mol%)	Gas Composition (mol%)	Molecular Weight	T_c (K)	P_c (bar)	ω	BIP with CO_2*	BIP with N_2*	BIP with H_2S*
CO_2	0	100	44	304.211	73.819	0.225	–	–	–
N_2	7.026	0	28	126.2	33.9	0.039	–0.02	–	–
H_2S	1.966	0	34.1	373.2	89.4	0.081	0.12	0.2	–
C_1	6.86	0	16	190.564	45.992	0.01141	0.125	0.031	0.1
C_2	10.559	0	30.1	305.322	48.718	0.10574	0.135	0.042	0.08
C_3	2.967	0	44.1	369.825	42.462	0.15813	0.15	0.091	0.08

*All the other BIPs are zero.

Table B-1—Fluid properties of acid gas sample and injection gas (Pan and Firoozabadi 1998; Li and Firoozabadi 2012). H_2S = hydrogen sulfide; N_2 = nitrogen.

Components	Oil Composition (mol%)	Gas Composition (mol%)	Molecular Weight	T_c (K)	P_c (bar)	ω	BIP with CO_2*
CO_2	1.69	100	44.01	304.2	73.76	0.225	–
C_1	17.52	0	16.043	174.44	46	0.008	0.085
C_{2-3}	22.44	0	37.9086	347.26	44.69	0.1331	0.085
C_{4-6}	16.73	0	68.6715	459.74	34.18	0.2358	0.085
C_{7-14}	24.22	0	135.0933	595.14	21.87	0.5977	0.104
C_{15-25}	12.16	0	261.103	729.98	16.04	0.9118	0.104
C_{26+}	5.24	0	479.6983	910.18	15.21	1.2444	0.104

*All the other BIPs are zero.

Table B-2—Fluid properties of Oil G sample and injection gas (Khan et al. 1992; Pan et al. 2019).

Components	Oil Composition (mol%)	Gas Composition (mol%)	Molecular Weight	T_c (K)	P_c (bar)	ω	BIP with CO_2*
CO_2	0.77	95.0	44.01	304.20	73.76	0.225	–
C_1	20.25	5.0	16.04	190.60	46.00	0.008	0.12
C_{2-3}	11.80	0.0	38.4	343.64	45.05	0.130	0.12
C_{4-6}	14.84	0.0	72.82	466.41	33.50	0.244	0.12
C_{7-14}	28.63	0.0	135.82	603.07	24.24	0.600	0.12
C_{15-24}	14.90	0.0	257.75	733.79	18.03	0.903	0.12
C_{25+}	8.81	0.0	479.95	923.20	17.26	1.229	0.12

*All the other BIPs are zero.

Table B-3—Fluid properties of NWE oil sample and injection gas (Khan et al. 1992; Okuno et al. 2010).

Components	Oil Composition (mol%)	Gas Composition (mol%)	Molecular Weight	T_c (K)	P_c (bar)	ω	BIP with CO_2*
CO_2	1.92	100.0	44.01	304.20	73.76	0.225	–
C_1	6.93	0.0	16.04	166.67	46.00	0.008	0.05
C_{2-3}	17.42	0.0	36.01	338.81	45.53	0.126	0.05
C_{4-6}	19.44	0.0	70.52	466.12	33.68	0.244	0.05
C_{7-16}	31.38	0.0	147.18	611.11	20.95	0.639	0.09
C_{17-29}	15.49	0.0	301.48	777.78	15.88	1.000	0.09
C_{30+}	7.42	0.0	562.81	972.22	15.84	1.281	0.09

*All the other BIPs are zero.

Table B-4—Fluid properties of JEMA oil sample and injection gas (Khan et al. 1992; Okuno et al. 2010).

Appendix C—Calculated PX Diagrams for the Four Fluid Mixtures

Figs. C-1 through C-4 show the PX phase diagrams for acid gas, Oil G, NWE oil, and JEMA oil. These diagrams are generated using the trust-region-optimization-based PT algorithm. Note that the temperatures of the four cases are 178.8, 307.59, 301.48, and 316.48 K, respectively. For each diagram, a total of 160,000 algorithm runs are involved. No single failure is found during these computations. Fig. C-1 shows the most complex phase diagram with three single-phase, three two-phase, and one three-phase regions under relatively low temperatures. For each diagram among Figs. C-2 through C-4, a large three-phase (i.e., three-phase vapor/liquid/liquid equilibria) region appears in the lower right. In such a three-phase vapor/liquid/liquid equilibrium for CO_2/oil mixtures, the first liquid phase is a lighter phase rich in CO_2, whereas the second liquid phase is a heavier phase rich in oil. For Figs. C-1 through C-4, it can be observed that the phase boundaries have fairly smooth and consistent shapes.
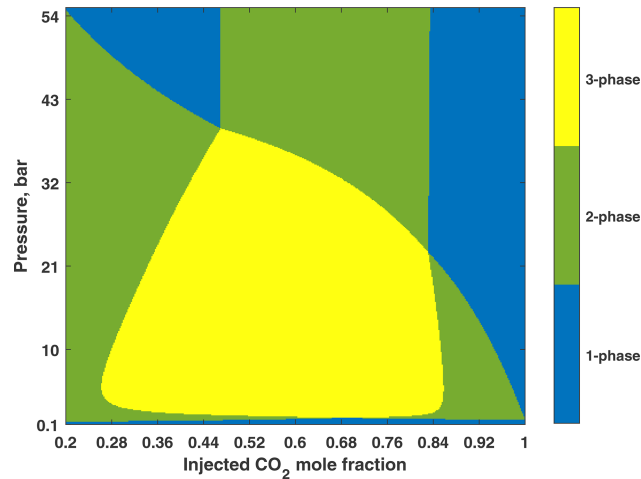
Fig. C-1—PX diagram generated using the multiphase PT algorithm for the acid sample mixed with CO_2 at 178.8 K. The graph is generated by multiphase equilibrium calculations over a mole fraction interval of 0.002 and a pressure interval of 0.1375 bar. A total of 160,000 equilibrium calculations are involved.
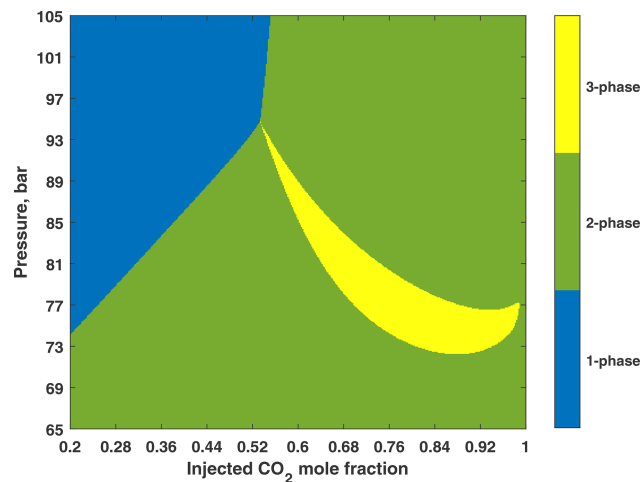
Fig. C-2—PX diagram generated using the multiphase PT algorithm for the Oil G sample mixed with the injection gas at 307.59 K. The graph is generated by multiphase equilibrium calculations over a mole fraction interval of 0.002 and a pressure interval of 0.1 bar. A total of 160,000 equilibrium calculations are involved.
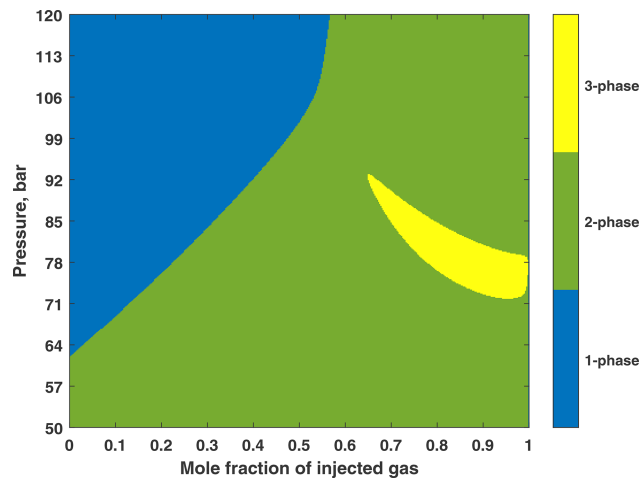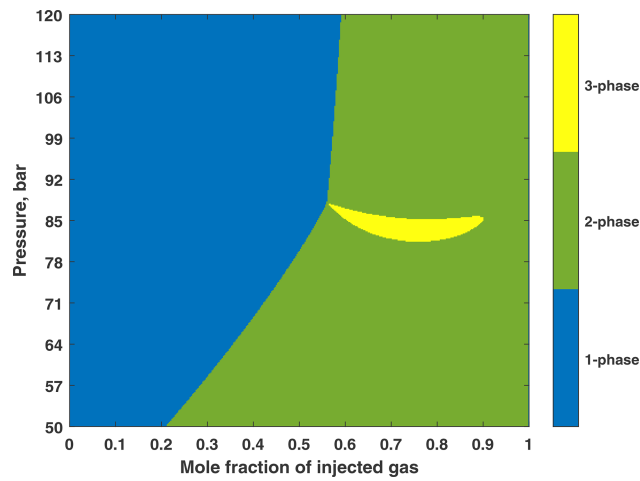
Fig. C-3—PX diagram generated using the multiphase PT algorithm for the NWE oil sample mixed with the injection gas at 301.48 K. The graph is generated by multiphase equilibrium calculations over a mole fraction interval of 0.0025 and a pressure interval of 0.175 bar. A total of 160,000 equilibrium calculations are involved.

Fig. C-4—PX diagram generated using the multiphase PT algorithm for the JEMA oil sample mixed with the injection gas at 316.48 K. The graph is generated by multiphase equilibrium calculations over a mole fraction interval of 0.0025 and a pressure interval of 0.175 bar. A total of 160,000 equilibrium calculations are involved.

Appendix D—Calculation Results for the JEMA Oil Sample and Injection Gas (Khan et al. 1992; Okuno et al. 2010)

Please see **Figs. D-1 through D-8**.
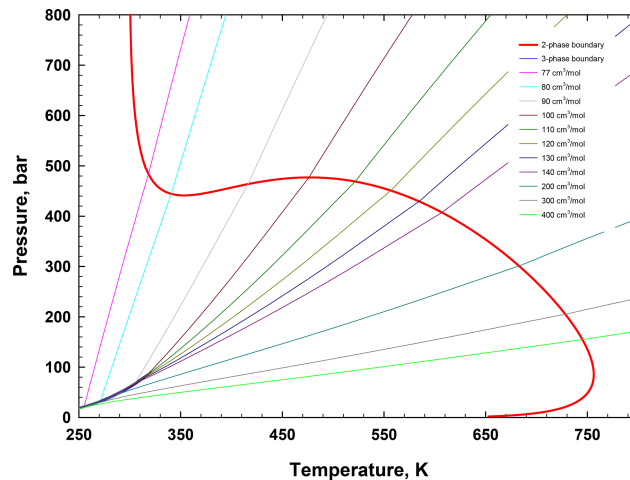
Fig. D-1—Two-phase and three-phase envelopes calculated for the JEMA oil mixed with 75-mol% injection gas as shown in Table B-4. The isochoric lines are also calculated with the proposed algorithm and drawn.
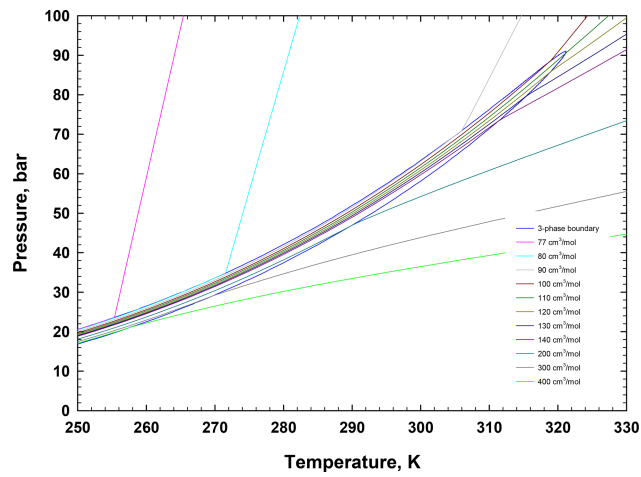
Fig. D-2—Close-up view of the three-phase boundary shown in Fig. D-1 with the isochoric lines passing through the three-phase region.
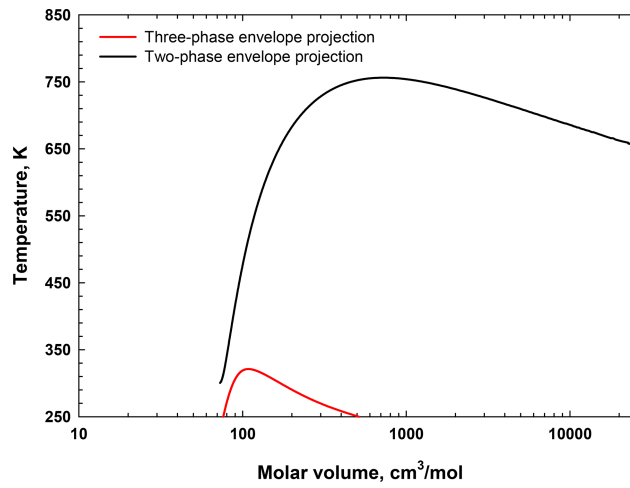

Fig. D-3—Projection of two-phase and three-phase envelopes in the temperature/volume space calculated for the JEMA oil mixed with 75-mol% injection gas.
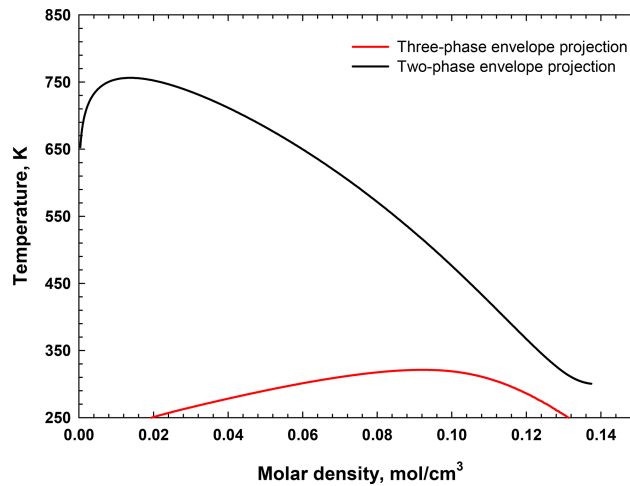

Fig. D-4—Projection of two-phase and three-phase envelopes in the temperature/density space calculated for the JEMA oil mixed with 75-mol% injection gas.
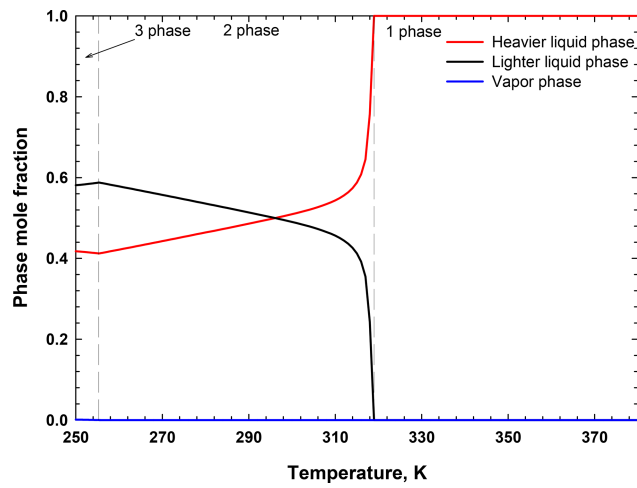
Fig. D-5—Variation of phase fractions vs. temperature along the isochore of 77 cm³/mol calculated for the JEMA oil mixed with 75-mol% injection gas.
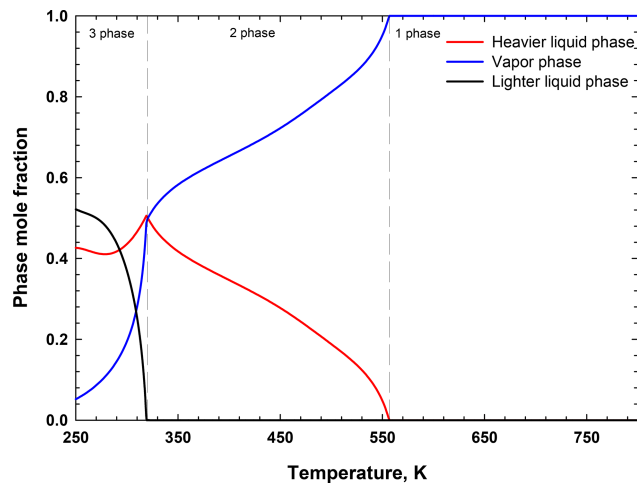

Fig. D-6—Variation of phase fractions vs. temperature along the isochore of 120 cm³/mol calculated for the JEMA oil mixed with 75-mol% injection gas.
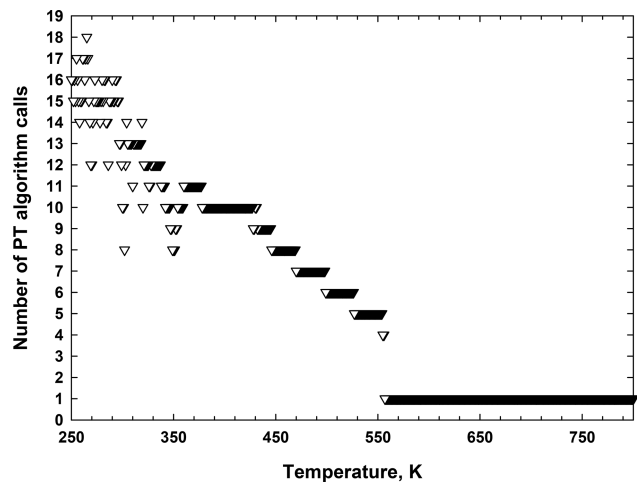

Fig. D-7—Number of PT algorithm calls in the implementation of the VT algorithm along the isochore of 120 cm³/mol for the JEMA oil mixed with 75-mol% injection gas.
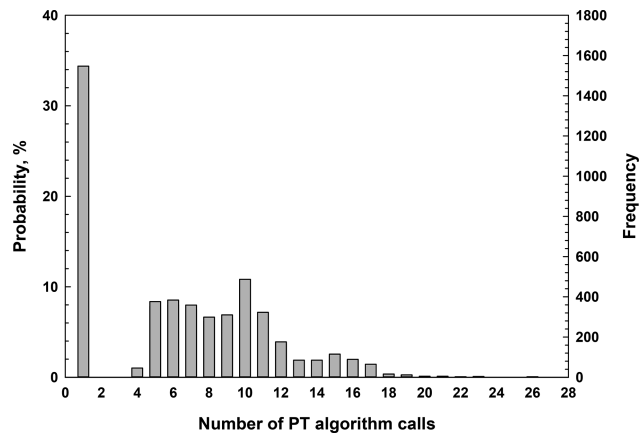
Fig. D-8—Statistical summary of the number of PT algorithm calls in the implementation of the VT algorithm along the isochores shown in Fig. D-1.